Human Molecular Genetics, 2021, Vol. 30, No. 17 1607–1617

https://doi.org/10.1093/hmg/ddab106
Advance Access Publication Date: 1 June 2021
General Article

GENERAL ARTICLE

PAK1 inhibition reduces tumor size and extends the lifespan of mice in a genetically engineered mouse model of Neurofibromatosis Type 2 (NF2)

Eric Hawley[1,†], Jeffrey Gehlhausen[1,†], Sofiia Karchugina[2], Hoi-Yee Chow[2], Daniela Araiza-Olivera[2], Maria Radu[2], Abbi Smith[3], Ciersten Burks[5], Li Jiang[3], Xiaohong Li[3], Waylan Bessler[3], Andrea Masters[4], Donna Edwards[1], Callie Burgin[3], David Jones[4], Charles Yates[5], D. Wade Clapp[1,3,*], Jonathan Chernoff[2] and Su-Jung Park[3]

[1]Department of Biochemistry and Molecular Biology, Indiana University School of Medicine, Indianapolis, IN 46202, USA, [2]Cancer Biology Program, Fox Chase Cancer Center, Philadelphia, PA 19111, USA, [3]Department of Pediatrics, Indiana University School of Medicine, Indianapolis, IN 46202, USA, [4]Clinical Pharmacology Analytical Core, Indiana University School of Medicine, Indianapolis, IN 46202, USA and [5]Department of Otolaryngology, Indiana University School of Medicine, Indianapolis, IN 46202, USA

*To whom correspondence should be addressed at: Department of Pediatrics, Riley Children's Hospital, 705 Riley Hospital Drive, Rm 5900, Indianapolis, IN 46202, USA. Tel: 3179447812; Email: dclapp@iu.edu

Abstract

Neurofibromatosis Type II (NF2) is an autosomal dominant cancer predisposition syndrome in which germline haploinsufficiency at the *NF2* gene confers a greatly increased propensity for tumor development arising from tissues of neural crest derived origin. *NF2* encodes the tumor suppressor, Merlin, and its biochemical function is incompletely understood. One well-established function of Merlin is as a negative regulator of group A serine/threonine p21-activated kinases (PAKs). In these studies we explore the role of PAK1 and its closely related paralog, PAK2, both pharmacologically and genetically, in Merlin-deficient Schwann cells and in a genetically engineered mouse model (GEMM) that develops spontaneous vestibular and spinal schwannomas. We demonstrate that PAK1 and PAK2 are both hyper activated in Merlin-deficient murine schwannomas. In preclinical trials, a pan Group A PAK inhibitor, FRAX-1036, transiently reduced PAK1 and PAK2 phosphorylation *in vitro*, but had insignificant efficacy *in vivo*. NVS-PAK1-1, a PAK1 selective inhibitor, had a greater but still minimal effect on our GEMM phenotype. However, genetic ablation of *Pak1* but not *Pak2* reduced tumor formation in our NF2 GEMM. Moreover, germline genetic deletion of *Pak1* was well tolerated, while conditional deletion of *Pak2* in Schwann cells resulted in significant morbidity and mortality. These data support the further development of PAK1-specific small molecule inhibitors and the therapeutic targeting of PAK1 in vestibular schwannomas and argue against PAK1 and PAK2 existing as functionally redundant protein isoforms in Schwann cells.

[†]Eric Hawley and Jeffrey Gehlhausen contributed equally to this work.

Received: January 25, 2021. **Revised:** April 7, 2021. **Accepted:** April 8, 2021

Introduction

Neurofibromatosis Type 2 (NF2) is an autosomal dominant cancer predisposition syndrome and NIH designated orphan disease. There are no approved therapeutics for use in affected patients. Patients with NF2 are born with a single functional copy of the tumor suppressor gene, *NF2*, and due to subsequent loss of heterozygosity, these individuals develop tumors of neural crest derived origin including meningiomas, ependymomas and most commonly, bilateral vestibular schwannomas (1–5). Although generally benign in nature, these tumors are often highly morbid due to their proximity to the central nervous system and their propensity to grow and compress vital structures in the brain and brainstem. Little is known about how Merlin functions as a tumor suppressor but previous studies have demonstrated that Merlin can directly interact with and prevent the activation of two of the isoforms of the group A serine/threonine p21-activated kinases, PAK1 and PAK2 (6,7). *PAK1* is a well-established oncogene which serves as a critical signaling node, regulating cell-proliferation, evasion of apoptosis and DNA damage repair, and is commonly amplified in a variety of human malignancies including solid tumors in brain, breast, liver, kidney and lung (8–11). *PAK2* is highly expressed in more than half of lymphoma, colorectal and ovarian cancers surveyed in the human protein atlas and higher expression of *PAK2* has been found to be a significant, clinically unfavorable prognostic marker in both pancreatic and prostate cancer (12). In addition, PAK1 activity levels have been shown to be elevated in human Schwannoma tumor tissues (13), and inhibition or reduced expression of Group 1 PAKs (PAK1, -2 and -3) has been shown to impede the growth of Merlin-deficient meningioma and Schwann cells *in vitro* and in xenografts (13–15).

We hypothesized that in the absence of Merlin's negative regulation, PAK1 and/or PAK2 may become constitutively active, leading *NF2*-deficient Schwann cells to form tumors in certain anatomical locations. Previously, a genetically engineered mouse model (GEMM) of NF2 was generated in which a 3.9 kb fragment of the *Periostin* promoter is utilized to drive expression of Cre recombinase resulting in the loss of expression of Merlin in Schwann cell progenitors during early maturation (16). These mice which are conditionally deficient in *Nf2* (*Nf2*-cKO) develop Schwann cell tumors in the vestibular-cochlear and trigeminal nerves as well as the spinal dorsal root ganglia (DRG) with 100% penetrance by 8 months of age. We undertook preclinical therapeutic trials in *Nf2*-cKO animals with both pan-PAK and PAK1 selective inhibitors. Then, utilizing genetic manipulation in these *Nf2*-cKO mice, we investigated the *in vivo* roles of PAK1 and PAK2 in Schwann cell tumor development. Our data demonstrate that PAK1 but not PAK2 plays a critical role in the formation and development of Merlin-deficient Schwann cell tumors. Deletion of *Pak1* but not *Pak2* reduced the average tumor size and extended the lifespan of the NF2 GEMM animals. These data argue that PAK1 and PAK2 have non-redundant functions as oncoproteins and that Merlin's role as a direct, negative regulator of PAK1 is critical to the tumor suppressive effects Merlin exerts in Schwann cells.

Results

FRAX-1036 is a potent inhibitor of PAK1/2 in Merlin-deficient Schwann cells *in vitro*

In vivo, PAK1 forms a homodimer in which the N-terminal regulatory domain of one monomer binds in trans to block the catalytic activity of a second monomer (17). Upon binding of RAC1 to the C-terminal p21 binding domain of PAK1, the homodimer disassociates and the PAK1 monomers are freed to autophosphorylate at T423 and S144 and initiate downstream signaling (18). Merlin is capable of binding to the P21 binding domain of PAK1, blocking the ability for RAC1 to trigger dissociation of the homodimer and holding PAK1 in its inactive conformation (6). Among its various substrates, PAK1 has been shown to phosphorylate MEK1 at S298 and RAF-1 at S338 and S339 to activate the RAF/MEK/ERK pathway, ILK at T173 and S246 to activate AKT signaling, PLK1 at S49 to drive the G2/M transition and Snail1/2 at S246 to activate WNT/b-catenin signaling (19–22) (Fig. 1A).

We first confirmed expression of PAK1 and PAK2 in trigeminal nerve tissue from the cKO mouse model. Total expression of PAK1 and PAK2 were similar in 10–12 month old Cre-positive and Cre-negative animals. PAK1 and PAK2 activation however, as measured by PAK1 and PAK2 autophosphorylation as well as phosphorylation of the downstream signaling proteins ERK1/2 and AKT were significantly increased in the Merlin conditionally deficient mice. Immunohistochemistry revealed that the activated pPAK1/2 localizes to Schwann cells within the Schwann cell tumors (Fig. 1C). PAK1 is activated under basal growth conditions as measured by phosphorylation of S144 in both the murine, Merlin-deficient MS02 Schwann cell line, and the human NF2 patient derived HEI-193 schwannoma cell line (Fig. 1D). Phosphorylation of PAK1 can be blocked by the Pan-Group A PAK inhibitor, FRAX-1036 (23). In Merlin-deficient HEI-193 cells, treatment with FRAX-1036 was correlated with a concentration-dependent reduction of both phosphorylation of PAK1 and downstream proliferative signaling as measured by ERK1/2 phosphorylation. In contrast, in Merlin-deficient murine Schwann cells (MS02), FRAX-1036 had a profound inhibitory effect on PAK1 activity, as assessed by autophosphorylation, but had much less effect on ERK1/2 phosphorylation. Despite this difference, FRAX-1036 potently reduced proliferation in the MS02 cells (IC50 of 162 nM) and in HEI-193 cells (IC50 of 1.6 μM) over 72 h (Fig. 1E). Expression of significant levels of PAK2 was not observed in these cells.

Treatment with *FRAX-1036* does not improve the NF2-like phenotype of Nf2-cKO mice

FRAX-1036 reduced proliferation of Merlin-deficient schwannoma cells *in vitro* so we designed a pre-clinical therapeutic trial to assess the efficacy of FRAX-1036 in slowing the growth of established schwannomas in our *Nf2*-cKO animals. We treated 8-month-old *Nf2*-cKO mice with a previously established maximum tolerated dose of 30 mg/kg daily of FRAX-1036. The *Nf2*-cKO mice uniformly develop Schwann cell hyperplasia between 5 and 6 months of age with fully penetrant frank schwannoma by 8 months. Untreated *Nf2*-cKO mice begin to die from tumor burden starting around 10 months of age. After 12 weeks of treatment there was no histological difference observed between the schwannomas of the FRAX-1036 and vehicle-treated control groups (Fig. 2A). The tumor size was similar between the two groups as measured by average DRG volume (Fig. 2B). Further, we observed no difference in either the magnitude or progression of sensorineural hearing between the FRAX-1036 and vehicle-treated animals (Fig. 2C).

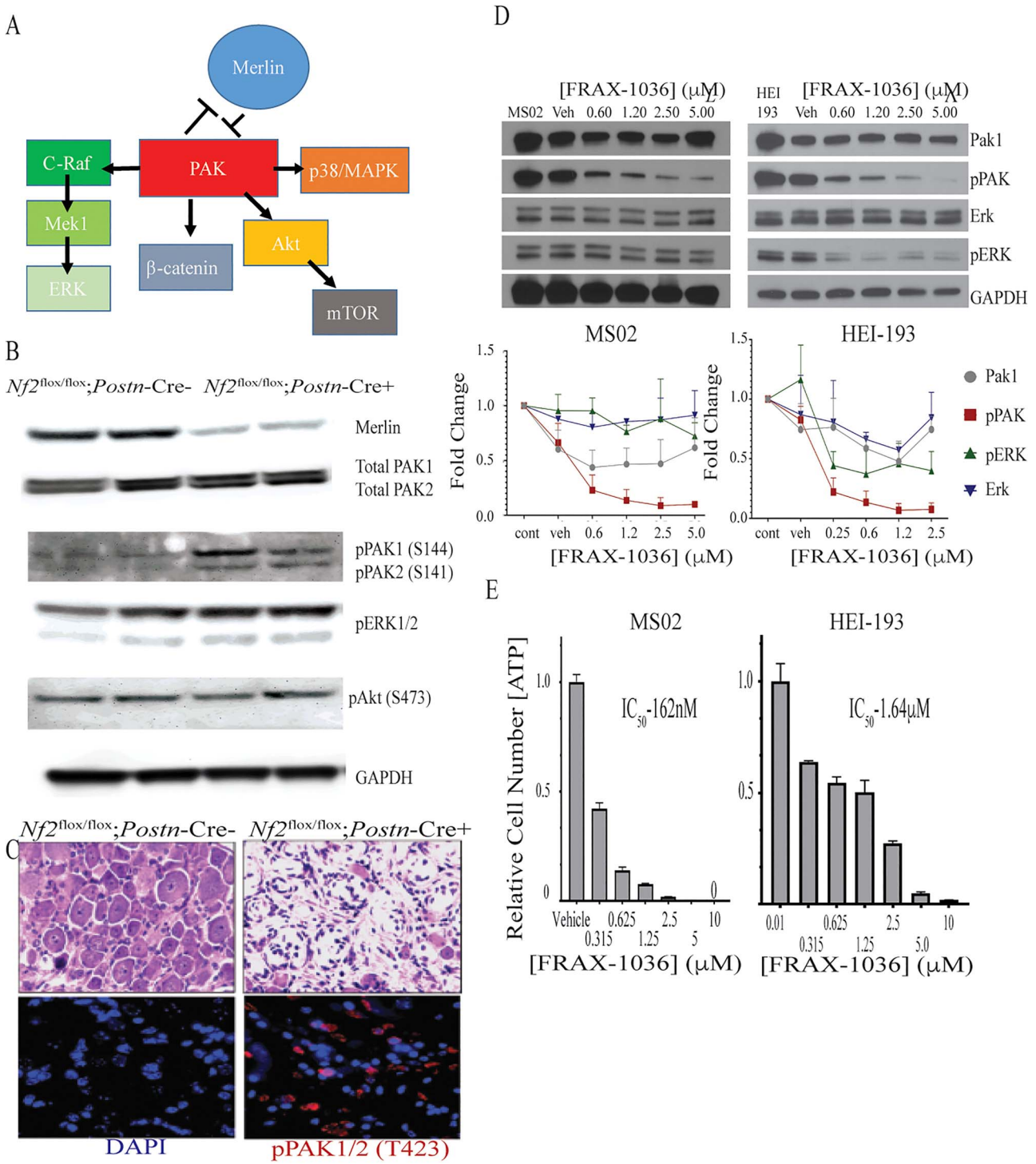

Figure 1. PAK1/2 activation state in Merlin-deficient murine schwannomas. (**A**) Schematic showing pathways known to be downstream of PAK1. (**B**) Immunoblot of trigeminal nerves from 10–12 month old mice. (**C**) Immunohistochemistry for phosphoPAK1/2 (T423) (Red) and DAPI (Blue) in DRG from 10-month old mice. Original magnification 60×. (**D**) Immunoblot showing a dose-dependent reduction in PAK1 phosphorylation upon treatment with FRAX-1036 in murine and human Merlin-deficient Schwann cells. Averaged dose response curves of two independent experiments (with two technical replicates each) are shown. All the proteins are normalized to loading control and their respective vehicle control. Error bars are shown as ± SEM. (**E**) 72-h proliferation assay showing a FRAX-1036 dose-dependent reduction in proliferation of murine and human Merlin-deficient Schwann cells. IC50 values calculated in GraphPad Prism via [inhibitor] *vs.* normalized response non-linear fit algorithm.

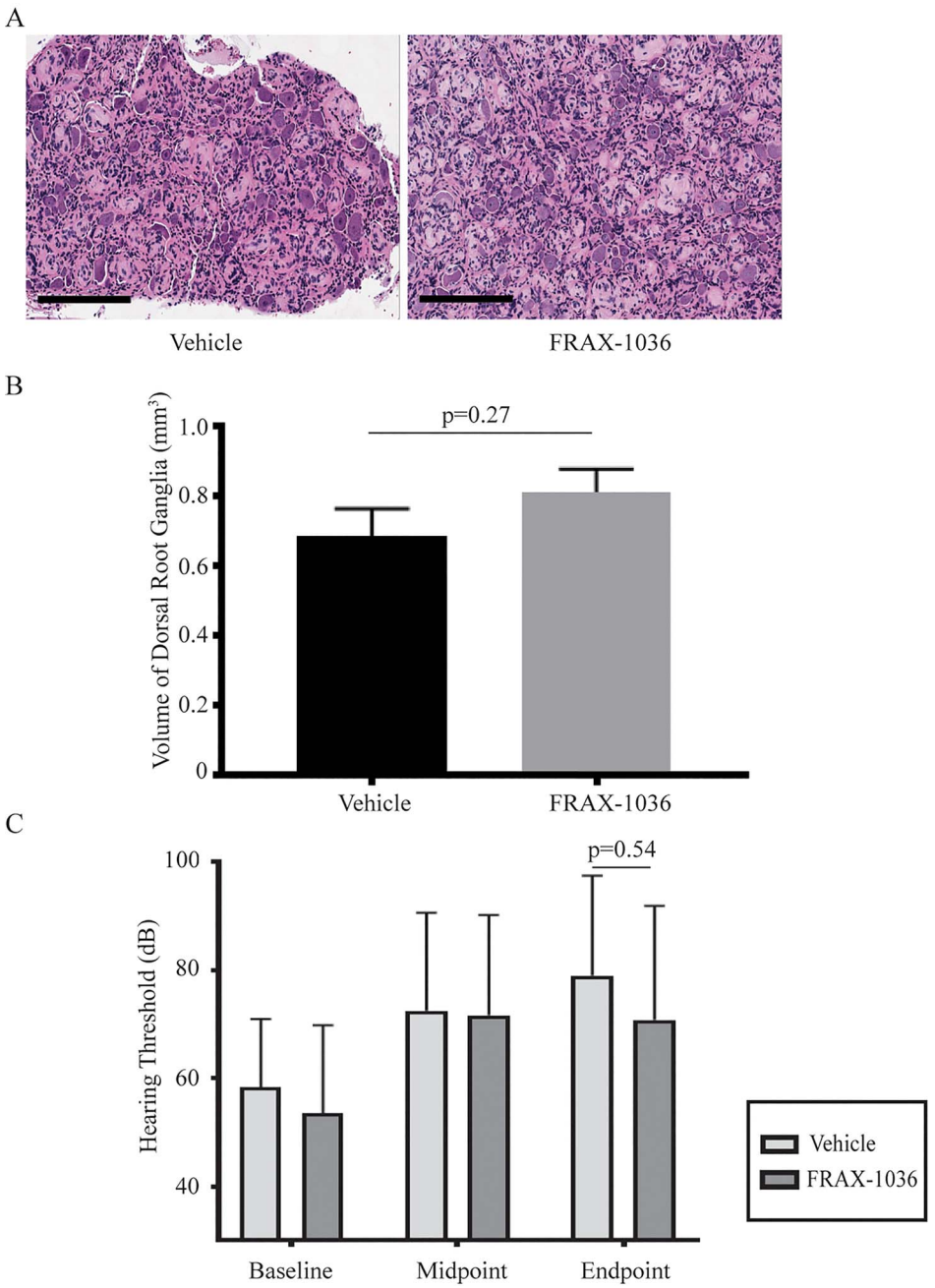

Figure 2. Tumor size/burden in FRAX-1036 treated mice. (**A**) H&E stained DRG from vehicle- and FRAX-treated mice. Original magnification 20×, scale bars =200 μM. (**B**) Average size of DRG in control and treatment groups. Four anatomically DRG were measured per mouse, n = 5 mice for vehicle group and n = 12 mice for FRAX-1036 treatment group. P = 0.27, students t-test error bars represent SEM. (**C**) ABR thresholds in FRAX- and vehicle-treated animals. Both ears in each animal were scored individually, n = 6 mice for vehicle-treated, n = 15 mice FRAX-treated, P = 0.54, two-way ANOVA with multiple comparisons, error bars represent SEM.

Treatment with *FRAX-1036* did not lead to durable inhibition of PAK1 *in vivo*

Administration of FRAX-1036 led to an average 1.7-fold decrease in pPAK1/2 staining in the Schwann cell tumors in DRG after 6 h. That difference was not statistically significant nor was it durable over the 24-h period between pharmacological administrations (Fig. 3A and B). Immunoblot analysis demonstrated a significant reduction in pPAK1/2 at 6 h post treatment (Fig. 3C). However, PAK activated pro-oncogenic pathways, including MEK, ERK, AKT, p38 and S6K, had reactivated to levels equal to or exceeding the vehicle control group by 6 h post drug administration, suggesting that FRAX-1036 as dosed did not lead to durable biological inhibition of PAK1/2.

PAK1 selective allosteric inhibitor NVS-PAK1-1 potently inhibits PAK1 phosphorylation *in vitro* and *in vivo*

To test whether more potent PAK inhibitors could provide a greater therapeutic effect, we acquired a second-generation pan-PAK inhibitor, G-5555, as well as a novel allosteric PAK1

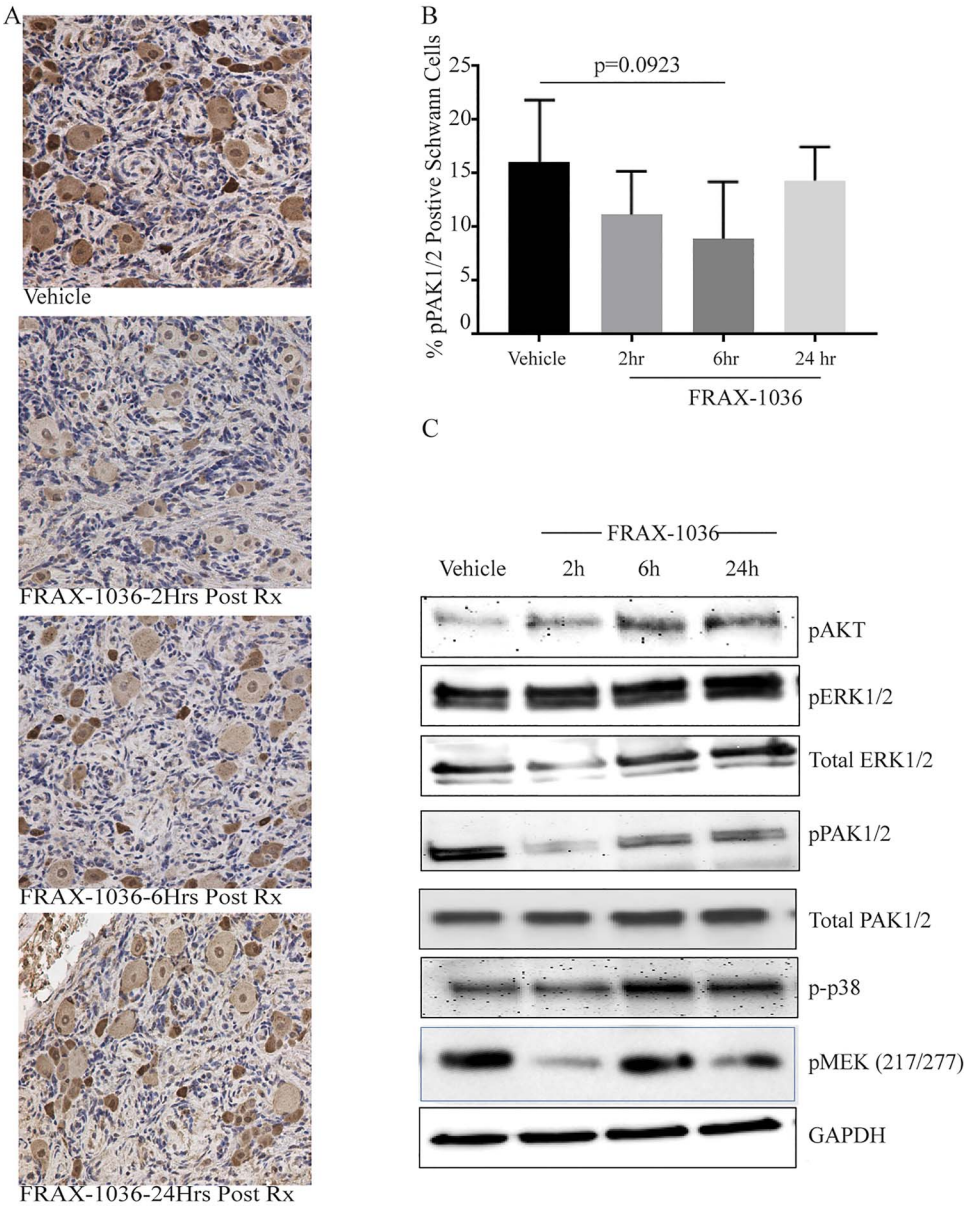

Figure 3. Pharmacodynamics FRAX-1036 treatment in tumor-bearing tissues. (**A**) Representative images of immunohistochemistry of pPAK1/2 (Thr423/402) in the DRG of treated mice at the specified time point after the final drug dose. Original magnification 20×. (**B**) Quantification of pPAK1/2^{+} Schwann cells in DRG schwannomas as measured by IHC. n = 4 mice at 2, 6 and 24 h post treatment. n = 5 mice for vehicle treatment. $P = 0.0923$, One-way ANOVA with Tukey's test, error these tumors were analyzed by immunoblot with the indicated antibodies. (**C**) At the indicated times, mice were sacrificed and tumors removed for signaling analysis. Lysates from these tumors were analyzed by immunoblot with the indicated antibodies.

inhibitor, NVS-PAK1-1 (24,25). More potent than FRAX-1036, G-5555 is mildly more selective for PAK1 than PAK2 and was poorly tolerated in our mice. Single 30 mg/kg doses proved to be lethal and when administered at 10 mg/kg, mice would develop progressive left ventricular hypertrophy with pronounced cardiac arrythmias within 10 days of treatment as measured by echocardiography (data not shown). NVS-PAK1-1 is almost 100× more selective for PAK1 than PAK2 and demonstrated excellent PAK1 inhibition *in vitro*. NVS-PAK1-1 potently inhibited PAK1 autophosphorylation in MS02 cells (Fig. 4A) and reduced the proliferation of MS02 and HEI-193 cells with an IC50 of 4.7 and 6.2 μM, respectively (Fig. 4B and C). These IC50 values were higher than what we had observed with FRAX-1036 in the same cell lines but the effects of NVS-PAK1-1, as opposed to what we had observed with FRAX-1036, appeared to be largely cytostatic and not cytotoxic, slowing the expansion of the two cell lines without triggering significant cell death.

Previous studies with NVS-PAK1-1 have been limited due to the very short half-life of the compound *in vivo*, likely because it is a dibenzodiazepine and is rapidly metabolized by the cytochrome P450 oxidase system. *In vitro*, NVS-PAK1-1 was rapidly degraded in the presence of human liver microsomes and that degradation could be strongly inhibited by the

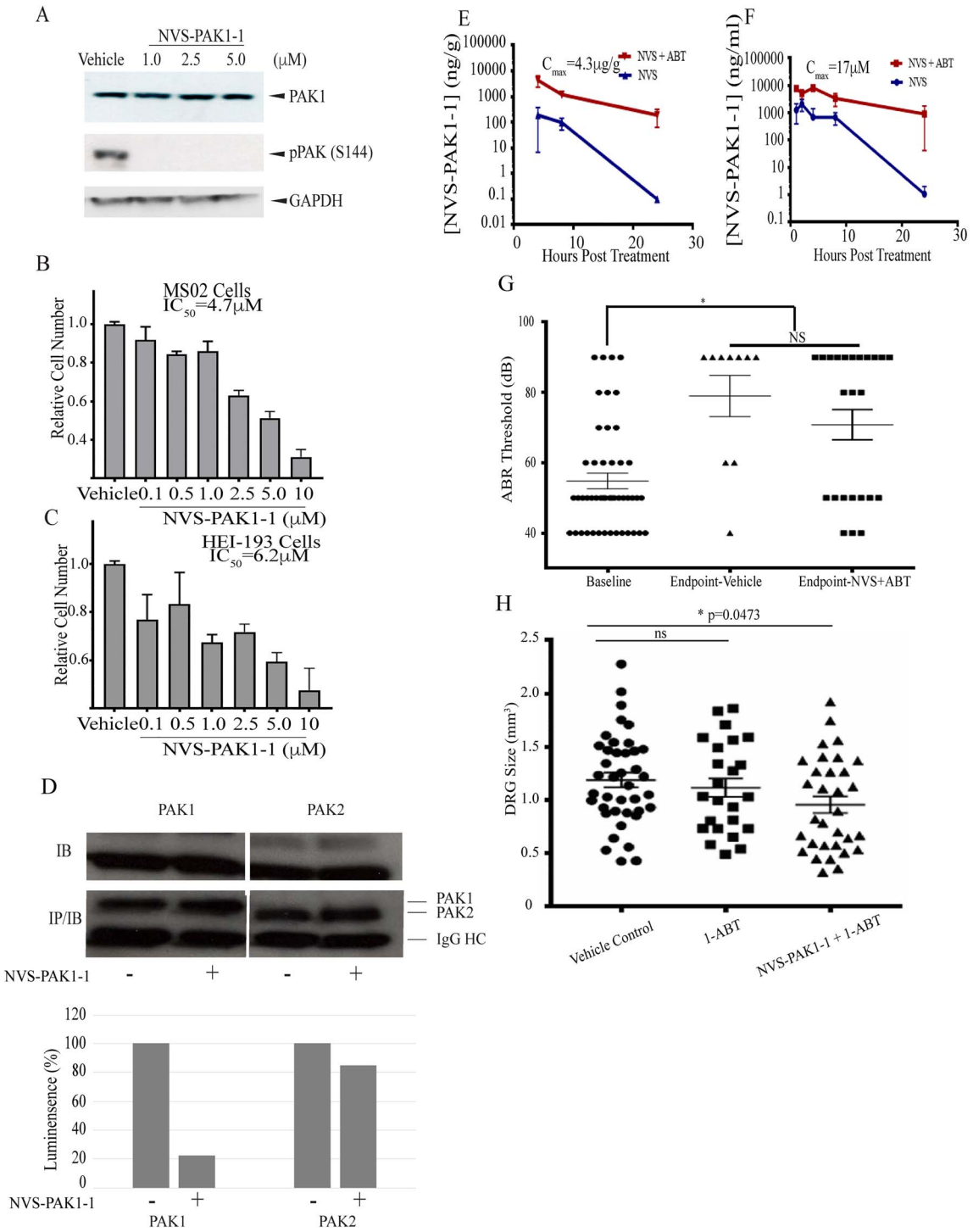

Figure 4. NVS-PAK1-1 inhibits Pak1 phosphorylation *in vitro* and *in vivo*. (**A**) 2 h treatment with NVS-PAK1-1 in MS02 cells. (**B**) 72 h proliferation assay in murine and (**C**) human Merlin-deficient schwannoma cell lines with IC50s of 4.7 and 6.2 μM, respectively, error bars represent SEM. IC50 values calculated in GraphPad Prism via the [inhibitor] vs normalized response non-linear fit algorithm. (**D**) IP kinase assay of Pak1 and Pak2, respectively, from tumors from control and NVS-PAK1-1 treated mice. An immunoblot of Pak1 and Pak2 immunoprecipitates, respectively, is shown in the top panel, as well as results of protein kinase assays using PAK-tide as substrate in the bottom panel. (**E**) Serum concentrations of NVS-PAK1-1 after 12 weeks of treatment with 30 mg/kg/qd NVS-PAK1-1 + 100 mg/kg 1-ABT along with a control of mice treated with a dose of NVS-PAK1-1 alone. Error bars represent SD. (**F**) Tissue concentrations of NVS-PAK1-1 after 12 weeks of treatment with 30 mg/kg/qd NVS-PAK1-1 + 100 mg/kg 1-ABT along with a control of mice treated with a dose of NVS-PAK1-1 alone. Error bars represent SD. (**G**) ABR thresholds in mice treated for 12 weeks with 30 mg/kg NVS-PAK1-1 + 1-ABT or the vehicle along with measurements at 4 months prior to initiation of therapy. Error bars represent SEM. Ears tested independently, baseline n = 19 mice, vehicle n = 6, NVS n = 13, $P < 0.05$, one way. (**H**) Quantification of average volume of spinal DRG. Four anatomically DRG were measured per mouse, n = 10 mice for vehicle group, n = 6 mice for 1-ABT alone treatment group, n = 8 mice for NVS-PAK1-1 + 1-ABT. $P = 0.0473$, one way ANOVA with Tukey's test, error bars represent SEM.

pharmacokinetic inhibitors, ritonavir, 1-aminobenzotriazole (1-ABT) and Ketoconazole. The use of pharmacokinetic inhibitors to boost the half-life of active pharmacologic agents is not novel where the antiretroviral protease inhibitor ritonavir has been used as part of combination therapies for both HIV and Hepatitic C in order to prolong the half-life of other agents in the treatment regimen.

To test the specificity of NVS-PAK-1-1 *in vivo*, we carried out an *in vitro* kinase assay using immunoprecipitated PAK1 and PAK2, respectively, from tumor from control and treated animals. Such assays are considered the 'gold-standard' for assessing kinase activity and provide a more quantitative readout than phosphoantibody blot analysis. The results shown in Figure 4D confirm that PAK1 but not PAK2 was significantly inhibited in drug-treated mice.

Based upon a dose escalation experiment with a combination of NVS-PAK1-1 and 1-ABT as a pharmacokinetic inhibitor, we settled on treating the mice with ½ the maximum tolerated dose. We then completed pharmacokinetics to quantify the concentration of NVS-PAK1-1 in serum and DRG tissue of mice treated with 30 mg/kg/qd of NVS-PAK1-1 and 100 mg/kg 1-ABT. That dosage was effective to achieve prolonged concentrations of the active compound in tumor-bearing tissues (Fig. 4E and F).

Treatment with NVS PAK1-1 reduces the average DRG size in Nf2-cKO mice

With the FRAX-1036 trial, we set up our preclinical studies to look at the effects of pan-PAK inhibition in slowing the growth of established tumors. But, because *Pak1* may function earlier and have a protective effect against the development of Schwann cell tumors age, Mice for the NVS-PAK1-1 trial were treated for 12 weeks starting at 4 months of age with 100 mg/kg ABT followed 2 h later by 30 mg/kg NVS-PAK1-1.

After 3 months of treatment, mice which received NVS-PAK1-1 did not exhibit a significant reduction in sensorineural hearing loss (Fig. 4G) but did have a modest, but statistically significant, reduction in average DRG volume compared with mice treated with 1-ABT alone or the vehicle control (Fig. 4H). To determine whether this limited signal is indicative of an incomplete but potentially meaningful drug target response, we undertook a series of genetic intercrosses to guide understanding of the value of PAKs as drug targets in schwannoma development and tumor therapy.

Germline deletion of Pak1 but not Pak2 reduces tumor formation and extends the lifespan of Nf2-cKO mice

In order to delineate the relative roles of *Pak1* and *Pak2* and determine whether inhibition of either Pak1 or Pak2 is sufficient to inhibit the formation or growth of Schwannomas, we undertook a series of genetic intercrosses wherein we interbred *Nf2*-cKO mice with mice deficient in *Pak1* ($Pak1^{-/-}$, *Pak1*-KO) or *Pak2* ($Pak2^{flox/flox}$, *Pak2*-cKO). $Pak2^{flox/flox}$ mice were used because, unlike $Pak1^{-/-}$ mice, germline deficiency in *Pak2* is lethal during development (26).

As tumors grow in the spinal DRG of *Nf2*-cKO mice, the overall volume of the DRGs expand, resulting in a significantly larger average DRG volume by 8 months of age. At 10 months of age, $Nf2^{flox/flox}$;$Pak1^{-/-}$; *Postn-Cre* (*Pak1*-DKO) mice maintained an average DRG size within normal limits (Fig. 5A). Furthermore, although these *Pak1*-DKO animals had evidence of Schwann cell proliferation and hyperplasia, there were no defined areas of Antoni A or Antoni B histology characteristic of schwannoma (Fig. 5B). Importantly, deletion of *Pak1* significantly extended the average lifespan of *Nf2*-cKO animals indicative of the long-term potential for both efficacy and tolerability of PAK1 inhibition (Fig. 5C). *Pak1*-DKO animals were protected against the development of sensorineural hearing loss at least out to 8 months of age, providing indirect evidence that vestibular schwannomas had not formed in these animals (Fig. 5D). In contrast to genetic loss of *Pak1*, mice intercrossed to have both a disruption of *Nf2* and *Pak2* ($Nf2^{flox/flox}$; $Pak2^{flox/flox}$) had no reduction in tumor size as compared to mice containing a disruption of *Nf2* only ($Nf2f^{lox/flox}$; *Postn Cre*) (Fig. 5A). Furthermore, the histology of the $Nf2^{flox/flox}$; $Pak2^{flox/flox}$ spinal nerves was pathologically similar to mice that contained a disruption of the *Nf2* alleles only (Fig. 5B). Given the gross pathological phenotypes observed in the spinal nerves of the $Nf2^{flox/flox}$; $Pak2^{flox/flox}$ mice, formal Kaplan Meier studies or ABR hearing testing were not pursued in that genotype.

Tissues from the *Pak1*-DKO animals displayed a significant reduction in MEK, ERK, p38 and b-catenin signaling (Fig. 5E). Due to the epitope similarity, the phospho-specific antibodies are not Group A PAK selective and bind PAK1, PAK2 and PAK3. PAK1 and PAK2 are different molecular weights and can be separated after electrophoresis on a denaturing gel. PAK1 and PAK3 are only one amino acid different in length and are not distinguishable from each other on immunoblots. This may account for the high levels of PAK phosphorylation observed in the trigeminal and brachial nerve plexi in PAK1 deficient animals. The neuron cell bodies avidly and non-specifically react with the secondary antibody we use for immunohistochemistry so we haven't been able to utilize IHC to localize PAK3 expression to the neurons in these tissues but we have not observed PAK3 expression in purified Merlin-deficient Schwann cell populations.

Discussion

It is well established that PAK1 and PAK2 are pathologically elevated in schwannomas and thus have been targets of interest. Previously PAK1 and PAK2 have generally been thought to be largely functionally redundant such that inhibition of both would be required to achieve any antitumoral response. However, our genetic data argue that *Pak1* but not *Pak2* negatively impacts tumor formation. These genetic data are functionally important because inhibition of PAK2 appears, at least in mice, to be profoundly cardiotoxic. Consequently, selective inhibition of PAK1 may be a viable strategy to prevent tumor formation while working to overcome the *in vivo* intolerability of pan-PAK inhibitors. This strategy may have application in other solid tumors as well (27).

Genetic deletion of *Pak1* led to a much more robust suppression of the NF2-like pathologies in our mice than did pharmacologic inhibition of PAK1 with NVS-PAK1-1. This difference in observed outcomes may be due to the fact that these two interventions are not true surrogates. PAK1 is never expressed in the mice harboring germline mutations in *Pak1* while it is functionally suppressed starting at 4 months of age in mice receiving NVS-PAK1-1. In our mice, tumor formation could theoretically start as early as embryonic day 12–13, after translation of the Cre recombinase and depletion of the preexisting Merlin. Inhibition of PAK1 activation with NVS-PAK1-1 at 4 months of age may have prevented further transformation of *Nf2*-deficient Schwann cells into tumors but may not alter the growth of tumors which had already become established. This hypothesis is supported by the binary response we saw with NVS-PAK1-1 treatment in which a greater percentage of DRGs in the mice appeared histologically normal but those DRGs which did bear tumors did not appear

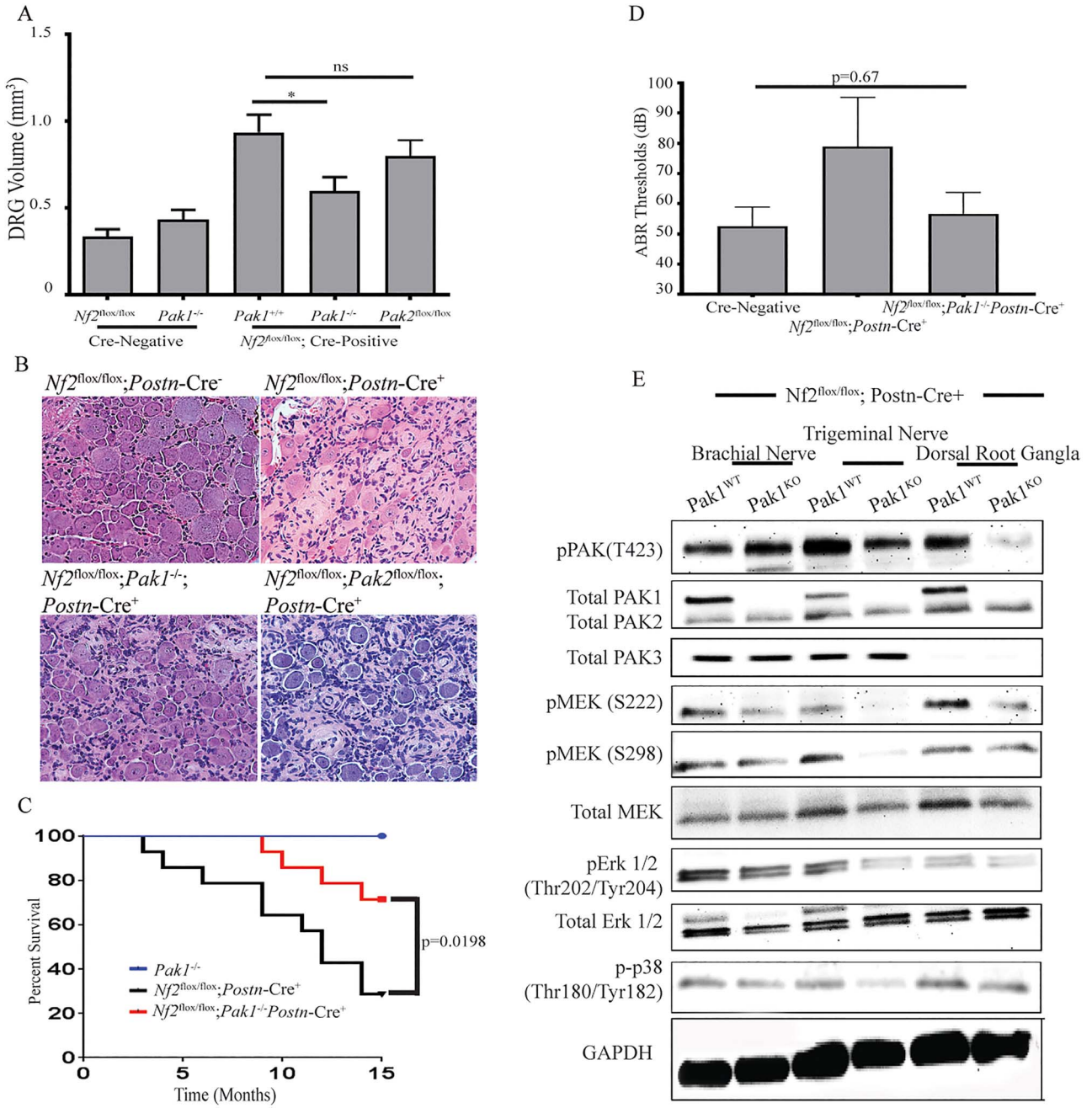

Figure 5. Effect of genetic ablation of PAK1 on DRG histology and formation of schwannoma in Merlin-deficient animals. 10-month-old Nf2-cKO and Nf2-cKO PAK1-KO animals were examined. (**A**) Quantification of average DRG volume. Four anatomically matched DRG were measured from each mouse. n = 5 mice/group for all groups except *Pak2* cDKO mice, n = 6 for *Pak2* cDKO mice. $P < 0.05$, one-way ANOVA with Tukey's test, error bars represent SEM. (**B**) Representative H&E sections of spinal dorsal root ganglia. Original magnification 20×. (**C**) Kaplan–Meier Curve of *Pak1* sufficient and deficient animals, n = 14 mice/group, $P = 0.0198$, Gehan–Breslow–Wilcoxon test. (**D**) ABR Thresholds at 8 months of age, both ears were tested independently on each mouse, Cre-Negatives n = 10 mice, $Nf2^{flox/flox}$; *Postn*-Cre^{+} n = 13 mice, $Nf2^{flox/flox}$; *Pak1*$^{-/-}$;*Postn*-Cre^{+} n = 5 mice. $P < 0.05$, one way ANOVA with Tukey's test, error bars represent SEM. (**E**) Mice were sacrificed and tissues removed for signaling analysis. Lysates from indicated tumors were analyzed by immunoblot with the indicated antibodies.

to be significantly inhibited by the treatment. Similarly, more mice in the NVS-PAK1-1 treated group had no detectable sensorineural hearing loss, but those mice which did have hearing loss developed a similar magnitude of hearing loss as the vehicle controls. In theory we could start treating mice at an early age and see if that generated a more profound drug response, but the actual practice of having to repeatedly gavage mice starting at 1–2 weeks of age rendered that approach unfeasible. Tumor development in humans is a more stochastic process driven by sporadic LOH. Tumors therefore are not likely to develop until much later, affording a longer time frame to initiate therapy and still achieve maximal effect.

Loss of Merlin in Schwann cells appears to be a rate-limiting step for tumor formation but much more work still needs to be done to define the downstream pathways which coordinate tumor growth and progression. In total, these studies provide

novel insight into the role of PAK1 in this process. PAK1 and PAK2 are not functionally redundant in Schwann cells and this work supports the further development of PAK1 selective inhibitors.

Materials and Methods

Animal study approval

Animal studies were conducted in accordance with and approved by the Institutional Animal Care and Use Committee of the respective university, the U.S. Department of Agriculture's Animal Welfare Act, and the Guide for the Care and Use of Laboratory Animals (IACUC #11406).

Statistical methods

Statistical analyses were performed in GraphPad Prism 7.02. As described in the text, analysis of variance (ANOVA) or Student's T-test were used to test for differences between samples and the Gehan–Breslow–Wilcoxon test was used to assess for differences in the Kaplan–Meier curve. Specific tests and significance levels can be found in the figures and figure legends.

Preparation of mouse nerve tissues for protein studies

Mice were sacrificed and freshly dissected nerve tissue was place in PBS on ice. Tissues were washed in cold PBS to remove any residual blood and then placed in 1.5 ml Eppendorf tubes containing cold xTractor Lysis buffer (Clontech) with Complete Protease inhibitor cocktail (Roche) and PhosSTOP EASYpack Phosphatase inhibitor cocktail (Roche). Tissues were minced with microdissection scissors and left to incubate on ice for 30 min. Tissues were then sonicated for 10 s and centrifuged at 16 100 RCF at 4°C for 15 min. The supernatant was collected and stored at −80°C for future use.

Immunoblot analysis

Protein concentrations for immunoblots were determined by the use of the Pierce BCA Protein Assay Kit (ThermoFisher). Equal aliquots of 20–30 µg protein were loaded and run on NuPAGE 412% Bis-Tris Gels (Invitrogen) and then transferred to PDVF membranes overnight. Membranes were blocked for 5 h in 5% milk and then incubated with primary antibody overnight. After washing, membranes were incubated with horseradish peroxidase linked anti-mouse IgG or anti-rabbit IgG (GE Healthcare, 1:5000) and visualized using SuperSignal Chemiluminescence substrate (ThermoFisher).

Kinase assays

Pak1 and Pak2 kinase assays were performed using an ADP-Glo™ system (Promega) with immunoprecipitates from excised tumors. Immunoprecipitates were washed and incubated at RT for 30 min in protein kinase buffer (50 mM Tris–HCl, pH 7.5, 10 mM $MgCl_2$, 1 mM DTT) containing 10 µM ATP and 0.25 mg/ml PAKtide (RRRLSFAEPG). Reactions were quenched using ADP-Glo™, then incubated at RT for 40 min. Kinase Detection Reagent was added to convert ADP to ATP and introduce luciferase and luciferin to detect ATP. Reactions were incubated at RT for 60 min and luminescence was measured with a plate-reading luminometer.

Histology and Immunohistochemistry

Freshly excised tissues were placed in 10% formalin and then embedded in paraffin and sectioned according to common procedures. The slides were deparaffinized in Xylenes and rehydrated through a series of graded alcohols to water. Antigen retrieval was performed in 10 mM sodium citrate buffer, pH 6, in a pressure cooker for 3 min. Endogenous peroxides were quenched in 0.3% hydrogen peroxide (10 min). Slides were blocked in 5% goat serum (1 h). Slides were incubated in PAK1 (Cell Signaling Technology, #2602) primary antibody diluted 1:100 (overnight at 4C), and then in biotinylated goat anti-rabbit secondary antibody (sigma B8895) diluted 1:800 (1 h). Slides were then incubated in VECTASTAIN ABC HRP (PK4000) (30 min), and then Vector DAB peroxidase substrate (sk-4100) was applied and slides were observed for color development. Slides were counterstained in Hematoxylin QS (Vector H3404), blued, dehydrated, and cover slipped. (All wash steps between different reagent applications were done with TBST for 5 min, three times).

Drug treatment of cell lines

HEI-193 and MS02 cell lines were seeded (0.3×10^6 cells per well) onto 6-well plates. The next day cells were treated with vehicle control DMSO (<0.01%) and FRAX-1036 (for MS02—0.6 uM, 1.2 uM, 2.5 uM, 5.0 uM; for HEI-193—0.25 uM, 0.6 uM, 1.2 uM, 2.5 uM), for 2 h. After 2 h plates were placed on ice, washed with ice-cold PBS, lysed with ice-cold RIPA buffer (50 mM Tris–HCl, pH 8.0, 150 mM NaCl, 0.1% SDS, 1% Triton X-100, 0.5 mM EGTA) supplemented with protease (Roche) and phosphatase (Sigma) inhibitors, scraped and incubated in cold tubes for 30 min on ice. Cell lysates were centrifuged at 18213 x g (12 700 rpm) at 4°C for 10 min, and the supernatant was used for determining protein concentration by Bradford assay (Bio-Rad). Standard immunoblotting procedures were followed. Membranes were blocked in 5% Milk diluted in TBST (TBS with 0.05% Tween 20) for 1 h. Protein ladder: Thermo Scientific PageRuler Plus Prestained Protein Ladder (#26619).

Software ImageJ (version 2.0.0) software was used to analyze and quantitate images.

Cell culture and Proliferation Assays

Murine *Nf2*$^{-/-}$schwannoma cells derived from a Schwann cell tumor which arose from an *Nf2*$^{flox/flox}$; *Postn*-Cre mouse or HEI-193 Human Schwann cells were plated in at 5000 cells/well in a 24-well plate containing 500 µl of Dulbecco's Modified Eagle Medium (DMEM, Gibco) containing 10% fetal bovine serum (FBS) (Sigma) and 2 mM L-Glutamine (Lonza) with the concentrations of the therapeutic as indicated in the figure. Cells were placed in ThermoForma Series II cell culture incubator for 72 h and proliferation was quantified via the CellTiter-Glo assay (Promega) following the manufacturers protocol. Human (HEI-193) and murine (MS02) immortalized schwannoma cells were maintained in Dulbecco's Modified Eagle medium (DMEM) supplemented with 10% FBS and 2 mM L-Glutamine (Lonza). GraphPad Prism (versions 7.0.4 and 8.0.2) built-in tests were used to analyze proliferation assays. For growth inhibition curves, data are the mean average of three independent experiments and error bars are represented as ± SEM.

In vivo Frax-1036 Treatment

Mice at ~8 months old were treated with 30 mg/kg Frax-1036 (C28H32ClN7O; M.W. 518.05) (Afraxis, CA) formulated in 20% (2-hydroxypropyl)-βcyclodextrin in 50 mM citrate buffer pH 3.0 daily for 12 weeks via oral gavage. Doses were chosen to provide minimum plasma concentrations of $\geq$0.5 mM at 24 h.

ABR Analysis

Auditory brainstem responses were measured at prior to enrollment, at the study midpoint, and just prior to sacrifice. Mice were anesthetized with Ketamine/Xylezene and placed into a custom apparatus with Faraday cage shielding and sound-dampening acoustic foam to attenuate electrical and sound interference. Click stimuli were presented at a rate of 21/s with stimuli presented in decreasing 10 dB increments from 90 to 30 dB via a closed-field speaker. Subdermal electrodes connected to a RA4PA Medusa Preamplifier and RZ6 auditory processor (Tucker Davis Technologies) performed the digital-audio conversions which were analyzed in the BioSigRZ application. Biological signals were band pass filtered above 3 Hz and below 3000 Hz. For mice in which no response was identified, a 90 dB threshold was recorded.

DRG Quantification

At the conclusion of the drug treatment, mice were sacrificed and then fixed for 48 h in 10% formalin. Carcasses were then transferred to 5% formalin/5% Formic acid for decalcification for 48 h. Whole nerve trees were then dissected out under a stereoscopic microscope. Four anatomically matched dorsal root ganglion were measured using the approximate volume of a spheroid, 0.52x $(\text{width})^2$ x length.

High-Performance Liquid Chromatography and Mass Spectrometry for Pharmacokinetics

High-performance liquid chromatography (HPLC) and Mass Spectrometry (MS) were performed by a core facility. Samples were acidified and extracted in hexane: ethyl acetate (50:50, v/v). After solvent evaporation, mobile phase (acetonitrile: 5 mM ammonium acetate; 70:30, v/v) was mixed with residual sample and injected into an Agilent 1290 HPLC system with an Eskigent Autosampler. Mass spectrometry was performed using an ABSciex 5500 Q-TRAP.

NVS-PAK1-1 Treatment

For the initial PK data, mice were treated with 100 mg/kg 1-ABT followed 2 h later by 100 mg/kg NVS-PAK1-1 in 60% PEG400/40% water via oral gavage. For the initial PD data mice were treated in a 6-week dose escalation where they received 100 mg/kg 1-ABT followed 2 h later by 10 mg/kg NVS-PAK1-1 in 60% PEG400/40% water for the first week with an increase of 10 mg/kg/week resulting in a final concentration of 100 mg/kg 1-ABT followed 2 h later by 60 mg/kg NVS-PAK1-1 in 60% PEG400/40% water via oral gavage prior to sacrifice. For the 12-week drug treatment and subsequent PK/PD data mice were treated PAK1-1 in 60% PEG-400/40% water via oral gavage. PK data were measured using the HPLC/MS approach described above.

Primary Antibody List

The following antibodies were used for Western Blotting experiments: cMYC (Cell Signaling Technology (CST) 5605), GAPDH (CST #5174), PAK1 (CST #2602), PAK2 (CST #2608), PAK1/2 (ThermoFisher PA5-38693), PAK3 (CST #2609), ERK1/2 (CST #9102), MEK (CST #4694), AKT (CST #4685), JNK (CST #9252), pPAK1/2 (S144/141) (CST #2606), pPAK1/2 (T423) (ThermoFisher PA38693), pMEK1/2 PS217/PS221 (CST #9154), pMEK PS298 (CST #98195), pAKT PS473 (CST #9271), pERK1/2 (CST #4370), pGSK3B PS9 (CST #9323), pp38 (CST #4511), pJNK (CST #9251), p70S6K PT389 (CST #9234).

Acknowledgements

This work was supported by the US Department of Defense [NF130108], and the National Institutes of Health [F30 DC041497-03].

Conflict of Interest statement. The authors have no conflicts of interest to declare.

References

1. Asthagiri, A.R., Parry, D.M., Butman, J.A., Kim, H.J., Tsilou, E.T., Zhuang, Z. and Lonser, R.R. (2009) Neurofibromatosis type 2. *Lancet*, **373**, 1974–1986.
2. Evans, D.G., Huson, S.M., Donnai, D., Neary, W., Blair, V., Newton, V. and Harris, R. (1992) A clinical study of type 2 neurofibromatosis. *Q. J. Med.*, **84**, 603–618.
3. Kanter, W.R., Eldridge, R., Fabricant, R., Allen, J.C. and Koerber, T. (1980) Central neurofibromatosis with bilateral acoustic neuroma: genetic, clinical and biochemical distinctions from peripheral neurofibromatosis. *Neurology*, **30**, 851–859.
4. Mautner, V.F., Lindenau, M., Baser, M.E., Hazim, W., Tatagiba, M., Haase, W., Samii, M., Wais, R. and Pulst, S.M. (1996) The neuroimaging and clinical spectrum of neurofibromatosis 2. *Neurosurgery*, **38**, 880–885 discussion 885-886.
5. Evans, D.G. (2009) Neurofibromatosis type 2 (NF2): a clinical and molecular review. *Orphanet J. Rare Dis.*, **4**, 16.
6. Kissil, J.L., Wilker, E.W., Johnson, K.C., Eckman, M.S., Yaffe, M.B. and Jacks, T. (2003) Merlin, the product of the Nf2 tumor suppressor gene, is an inhibitor of the p21-activated kinase, Pak1. *Mol. Cell*, **12**, 841–849.
7. Kissil, J.L., Johnson, K.C., Eckman, M.S. and Jacks, T. (2002) Merlin phosphorylation by p21-activated kinase 2 and effects of phosphorylation on merlin localization. *J. Biol. Chem.*, **277**, 10394–10399.
8. Eswaran, J., Li, D.Q., Shah, A. and Kumar, R. (2012) Molecular pathways: targeting p21-activated kinase 1 signaling in cancer–opportunities, challenges, and limitations. *Clin. Cancer Res.*, **18**, 3743–3749.
9. Shrestha, Y., Schafer, E.J., Boehm, J.S., Thomas, S.R., He, F., Du, J., Wang, S., Barretina, J., Weir, B.A., Zhao, J.J. *et al.* (2012) PAK1 is a breast cancer oncogene that coordinately activates MAPK and MET signaling. *Oncogene*, **31**, 3397–3408.
10. Ye, D.Z. and Field, J. (2012) PAK signaling in cancer. *Cell Logist.*, **2**, 105–116.
11. Motwani, M., Li, D.Q., Horvath, A. and Kumar, R. (2013) Identification of novel gene targets and functions of p21-activated kinase 1 during DNA damage by gene expression profiling. *PLoS One*, **8**, e66585.

12. Uhlen, M., Fagerberg, L., Hallstrom, B.M., Lindskog, C., Oksvold, P., Mardinoglu, A., Sivertsson, A., Kampf, C., Sjostedt, E., Asplund, A. *et al.* (2015) Proteomics. Tissue-based map of the human proteome. *Science*, **347**, 1260419.
13. Yi, C., Wilker, E.W., Yaffe, M.B., Stemmer-Rachamimov, A. and Kissil, J.L. (2008) Validation of the p21-activated kinases as targets for inhibition in neurofibromatosis type 2. *Cancer Res.*, **68**, 7932–7937.
14. Chow, H.Y., Dong, B., Duron, S.G., Campbell, D.A., Ong, C.C., Hoeflich, K.P., Chang, L.S., Welling, D.B., Yang, Z.J. and Chernoff, J. (2015) Group I Paks as therapeutic targets in NF2-deficient meningioma. *Oncotarget*, **6**, 1981–1994.
15. Licciulli, S., Maksimoska, J., Zhou, C., Troutman, S., Kota, S., Liu, Q., Duron, S., Campbell, D., Chernoff, J., Field, J. *et al.* (2013) FRAX597, a small molecule inhibitor of the p21-activated kinases, inhibits tumorigenesis of neurofibromatosis type 2 (NF2)-associated schwannomas. *J. Biol. Chem.*, **288**, 29105–29114.
16. Gehlhausen, J.R., Park, S.J., Hickox, A.E., Shew, M., Staser, K., Rhodes, S.D., Menon, K., Lajiness, J.D., Mwanthi, M., Yang, X. *et al.* (2015) A murine model of neurofibromatosis type 2 that accurately phenocopies human schwannoma formation. *Hum. Mol. Genet.*, **24**, 1–8.
17. Parrini, M.C., Lei, M., Harrison, S.C. and Mayer, B.J. (2002) Pak1 kinase homodimers are autoinhibited in trans and dissociated upon activation by Cdc42 and Rac1. *Mol. Cell*, **9**, 73–83.
18. Mayhew, M.W., Jeffery, E.D., Sherman, N.E., Nelson, K., Polefrone, J.M., Pratt, S.J., Shabanowitz, J., Parsons, J.T., Fox, J.W., Hunt, D.F. *et al.* (2007) Identification of phosphorylation sites in betaPIX and PAK1. *J. Cell Sci.*, **120**, 3911–3918.
19. Beeser, A., Jaffer, Z.M., Hofmann, C. and Chernoff, J. (2005) Role of group A p21-activated kinases in activation of extracellular-regulated kinase by growth factors. *J. Biol. Chem.*, **280**, 36609–36615.
20. Acconcia, F., Barnes, C.J., Singh, R.R., Talukder, A.H. and Kumar, R. (2007) Phosphorylation-dependent regulation of nuclear localization and functions of integrin-linked kinase. *Proc. Natl. Acad. Sci. U. S. A.*, **104**, 6782–6787.
21. Maroto, B., Ye, M.B., von Lohneysen, K., Schnelzer, A. and Knaus, U.G. (2008) P21-activated kinase is required for mitotic progression and regulates Plk1. *Oncogene*, **27**, 4900–4908.
22. Yang, Z., Rayala, S., Nguyen, D., Vadlamudi, R.K., Chen, S. and Kumar, R. (2005) Pak1 phosphorylation of snail, a master regulator of epithelial-to-mesenchyme transition, modulates snail's subcellular localization and functions. *Cancer Res.*, **65**, 3179–3184.
23. Koval, A.B. and Wuest, W.M. (2016) An optimized synthesis of the potent and selective Pak1 inhibitor FRAX-1036. *Tetrahedron Lett.*, **57**, 449–451.
24. Ndubaku, C.O., Crawford, J.J., Drobnick, J., Aliagas, I., Campbell, D., Dong, P., Dornan, L.M., Duron, S., Epler, J., Gazzard, L. *et al.* (2015) Design of Selective PAK1 inhibitor G-5555: improving properties by employing an unorthodox low-pK a polar moiety. *ACS Med. Chem. Lett.*, **6**, 1241–1246.
25. Karpov, A.S., Amiri, P., Bellamacina, C., Bellance, M.H., Breitenstein, W., Daniel, D., Denay, R., Fabbro, D., Fernandez, C., Galuba, I. *et al.* (2015) Optimization of a Dibenzodiazepine hit to a potent and selective allosteric PAK1 inhibitor. *ACS Med. Chem. Lett.*, **6**, 776–781.
26. Radu, M., Lyle, K., Hoeflich, K.P., Villamar-Cruz, O., Koeppen, H. and Chernoff, J. (2015) p21-activated kinase 2 regulates endothelial development and function through the Bmk1/Erk5 pathway. *Mol. Cell. Biol.*, **35**, 3990–4005.
27. Chow, H.Y., Jubb, A.M., Koch, J.N., Jaffer, Z.M., Stepanova, D., Campbell, D.A., Duron, S.G., O'Farrell, M., Cai, K.Q., Klein-Szanto, A.J. *et al.* (2012) p21-activated kinase 1 is required for efficient tumor formation and progression in a Ras-mediated skin cancer model. *Cancer Res.*, **72**, 5966–5975.